RSC Advances

PAPER

View Article Online
View Journal | View Issue

Published on 09 May 2014. Downloaded by Michigan State University on 23/01/2016 03:02:08.

Cite this: *RSC Adv.*, 2014, **4**, 26729

Anomalous effects of water flow through charged nanochannel membranes†

Meng Yang, Xiaohai Yang,* Qing Wang, Kemin Wang,* Xin Fan, Wei Liu, Xizhen Liu, Jianbo Liu and Jin Huang

Received 1st April 2014
Accepted 9th May 2014

DOI: 10.1039/c4ra02856b

www.rsc.org/advances

A nanoscale understanding of water transport is crucial to gaining fundamental insights into biological systems and improving the design of engineered systems. Herein, anomalous effects of water flow were observed in our experiment by measuring the net flux of water through charged nanochannel membranes that separated pure water from an electrolyte solution. The direction and flux of water transport can be controlled as a function of nanochannel surface charge, electrolyte concentration and electrolyte type. For some electrolyte types in the proper concentration range, the net flux of water transport was from the electrolyte solution to the pure water, which is an anomalous osmosis phenomenon and violates van't Hoff's law. In order to explain this anomalous effect, a concise model was put forward. According to the model, the direction and flux of water transport were the result of combining concentration diffusion with induced electroosmosis under certain electrolyte gradients. In addition, neutral molecule transport, and ionic species separation through charged nanochannel membranes can also be modulated by adjusting the electrolyte gradient. These results suggest that polyelectrolyte modified nanochannel membranes have good potential for application as a kind of nanovalve under an electrolyte gradient.

1 Introduction

Studies of mass transport in nanoscale will contribute to our understanding of underlying transport mechanisms and aid in developing nanofluidic devices.[1–5] Mass transport on the nanoscale differs greatly from that at a bulk-scale, since various surface or interfacial forces including steric interactions, van der Waals forces and electrostatic forces become important due to the large surface-to-volume ratios.[6–9] For example, in nanochannels, the channel dimensions are narrowed to electrical double layer (EDL) thickness.[10] Usually, the overlapping of EDL is very significant, leading to various unique properties including ion selectivity,[11–13] local ion depletion/enrichment,[14–16] active gated control of ions/molecules,[17–23] ionic current rectification[24–28] and energy conversion from streaming current.[29–31] Thus, novel transport properties on the nanoscale are expected to emerge from a combination of the strong confinement and the unique surface properties.

In recent years, with advances in processing technology for artificial nanochannel preparation, as well as some new means of detection in experiments, there have been some interesting reports on mass transport phenomena in nanoscale. Holt *et al.* reported fast mass transport through sub-2-nanometer carbon nanotubes.[32] They found that water permeabilities in carbon nanotubes with diameters of less than 2 nm are several orders of magnitude higher than those of commercial polycarbonate membranes, despite having pore sizes an order of magnitude smaller. Chmiola *et al.* found that decreasing the pore size to less than 1 nm led to an anomalous increase in carbon capacitance.[33] Lee *et al.* observed water flow enhancement in hydrophilic nanochannels.[34] Duan *et al.* reported that the mobility of ions restricted in 2 nm hydrophilic nanochannels was faster than that in bulk phase, and proton mobility was increased four times over the bulk value at low concentrations.[35] Chinen *et al.* observed that proton mobility was enhanced in the extended-nanospace channels from 570 nm to 180 nm by using a pH-sensitive fluorescent probe to monitor the proton diffusion in the extended-nanospace channels.[36] This phenomenon cannot be explained by the change in the viscosity of water because water confined in the extended nanospaces has a higher viscosity compared with bulk water.[37] Chen *et al.* reported the anomalous diffusion of electrically neutral molecules in charged nanochannels. For the first time, they found that the diffusion flux of phenol, a neutral molecule, varied with the ionic strength in 20 nm alumina

State Key Laboratory of Chemo/Biosensing and Chemometrics, College of Chemistry and Chemical Engineering, Key Laboratory for Bio-Nanotechnology and Molecular Engineering of Hunan Province, Hunan University, Changsha 410082, P. R. China. E-mail: kmwang@hnu.edu.cn; yangxiaohai@hun.edu.cn; Fax: +86-731-88821566; Tel: +86-731-88821566

† Electronic supplementary information (ESI) available: Number of deposited *n*(PSS/PAH) multilayers, SEM images of *n*(PSS/PAH) multilayers, TEM images of 3.5(PSS/PAH) nanotubes, experimental system used to measure the liquid levels, ionic conductivity and diffusion coefficient. See DOI: 10.1039/c4ra02856b

Published on 09 May 2014. Downloaded by Michigan State University on 23/01/2016 03:02:08.

nanochannels.[38] These anomalous transport phenomena mostly stem from interactions between the transported mass and the nanochannel walls.

Numerical simulation also contributes to our understanding of mass transport at the nanoscale. Several recent numerical studies have showed that anomalous osmosis, *i.e.* water flow through charged nanochannels from a higher electrolyte concentration to a lower electrolyte concentration, can occur.[39–41] This inference is interesting and can offer some basic explanations of the translocation of liquids across biological membranes, since some phenomena of liquid transport through biological membranes cannot be explained on the basis of the concept of normal van't Hoff osmosis.[42,43] However, presently experimental investigations based on charged nanochannels are still scarce. Thus, it is important to investigate mass transport through charged nanochannels experimentally to clarify the anomalous water transport mechanisms at the nanoscale.

Here, we provide an experimental study of the anomalous osmosis phenomenon for artificially charged nanochannel membranes. The charged nanochannel membranes were fabricated by depositing layer-by-layer assembled polyelectrolyte multilayers comprising poly(allylamine hydrochloride) (PAH) and poly(sodium 4-styrenesulfonate) (PSS) in 100 nm track-etched polycarbonate membranes (TEPC) (see Fig. S1†). A concise model was established to describe the conditions of anomalous osmosis. It pointed out that the direction and net flux of water transport were determined by concentration diffusion and induced electroosmosis. When the directions of concentration diffusion and induced electroosmosis were opposite, anomalous osmosis could occur under certain electrolyte gradients. The direction and net flux of water transport were investigated under different conditions, including electrolyte concentrations, electrolyte types and charge of the nanochannel membranes. The results showed that the inferences of model were consistent with experimental data. In addition, according to the model, neutral molecular transport and ionic species separation can be modulated by adjusting the electrolyte gradient. To demonstrate this, the electrically neutral molecule (phenol) and ionic species (methylviologen (MV^{2+}) dichloride and 1,5-naphthalene disulfonate (NDS^{2-}) disodium salt) were selected as models.

2 Model of transport

To explore the transport of water through the charged nanochannel membranes under an electrolyte gradient, a transport model was put forward. As shown in Fig. 1, water transport is composed of concentration diffusion and induced electroosmosis, the net flux of water transport is the net result of the two parts. According to differences in nanochannel surface charge and electrolyte type, the transport model can be divided into four kinds of situations, which are shown in Fig. 1a–d. To illustrate our model, we employed Fig. 1a as an example, *i.e.* a negatively charged nanochannel membrane connecting two half-cells which contained an electrolyte solution and pure water, respectively.

Obviously, according to van't Hoff's law, there would be water transportation from the pure water to electrolyte solution, which is induced by concentration diffusion. Such water transport is represented by the green arrow pointing left in Fig. 1a, marked as F_{cd}.

In addition, water transport is also caused by induced electroosmosis. However, the generation of induced electroosmosis is more complex than F_{cd}. As shown in Fig. 1a, according to the two-region model mentioned by Chen *et al.*, an electrostatic interaction region and a free transport region exist in the nanochannel.[38,44]

For a negatively charged nanochannel, the channel surface can attract cations (M^+), forming an electric double layer (EDL), and repel anions (A^-) due to the electrostatic interactions. Diffusion of anions (A^-) through the nanochannels mainly occurs in the free transport region under the electrolyte gradient. Since the diffusion coefficient of the anion (A^-) is larger than that of the cation (M^+), the anions can pass channel more quickly. This causes anions (A^-) to accumulate faster in the pure water half-cell. As a result, a membrane diffusional potential is formed between the two half-cells. The membrane diffusional potential which, acting on the cations accumulated in the EDL, induces water transport which is referred to as induced electroosmosis. Such water transport is represented by the orange arrow pointing right in Fig. 1a, marked as F_{ie}. The direction of induced electroosmosis is towards the pure water half-cell.

As shown in Fig. 1a, the directions of F_{cd} and F_{ie} are opposite. If F_{ie} is larger than F_{cd}, the net result is that water transport from the electrolyte solution to pure water, and therefore an anomalous osmosis phenomenon, may be observed. Therefore, if we change the electrolyte type and nanochannel surface charge, this anomalous osmosis phenomenon can be controlled.

As shown in Fig. 1b, for the negatively charged nanochannel, if the diffusion coefficient of the cation (M^+) is larger than that of the anion (A^-), the direction of F_{cd} is the same as the direction of F_{id}. Water is always transported from the pure water toward the electrolyte solution. Anomalous osmosis phenomena cannot be observed.

As shown in Fig. 1c, for the positively charged nanochannel, if the diffusion coefficient of the anion (A^-) is larger than that of the cation (M^+), the direction of F_{cd} is the same as the direction of F_{id}. Water is always transported from the pure water toward the electrolyte solution. Anomalous osmosis phenomena cannot be observed.

As shown in Fig. 1d, for the positively charged nanochannel, if the diffusion coefficient of the cation (M^+) is larger than that of the anion (A^-), the direction of F_{cd} is opposite to the direction of F_{id}. The anomalous osmosis phenomenon may be observed.

In order to provide evidence to prove these four inferences from the model, the net flux and direction of water transport were investigated by an experimental approach under different conditions, including electrolyte concentrations, electrolyte types and nanochannel surface charge. The setup for the water transport experiment is shown in Fig. 2 and S4.†

 This journal is © The Royal Society of Chemistry 2014

Published on 09 May 2014. Downloaded by Michigan State University on 23/01/2016 03:02:08.

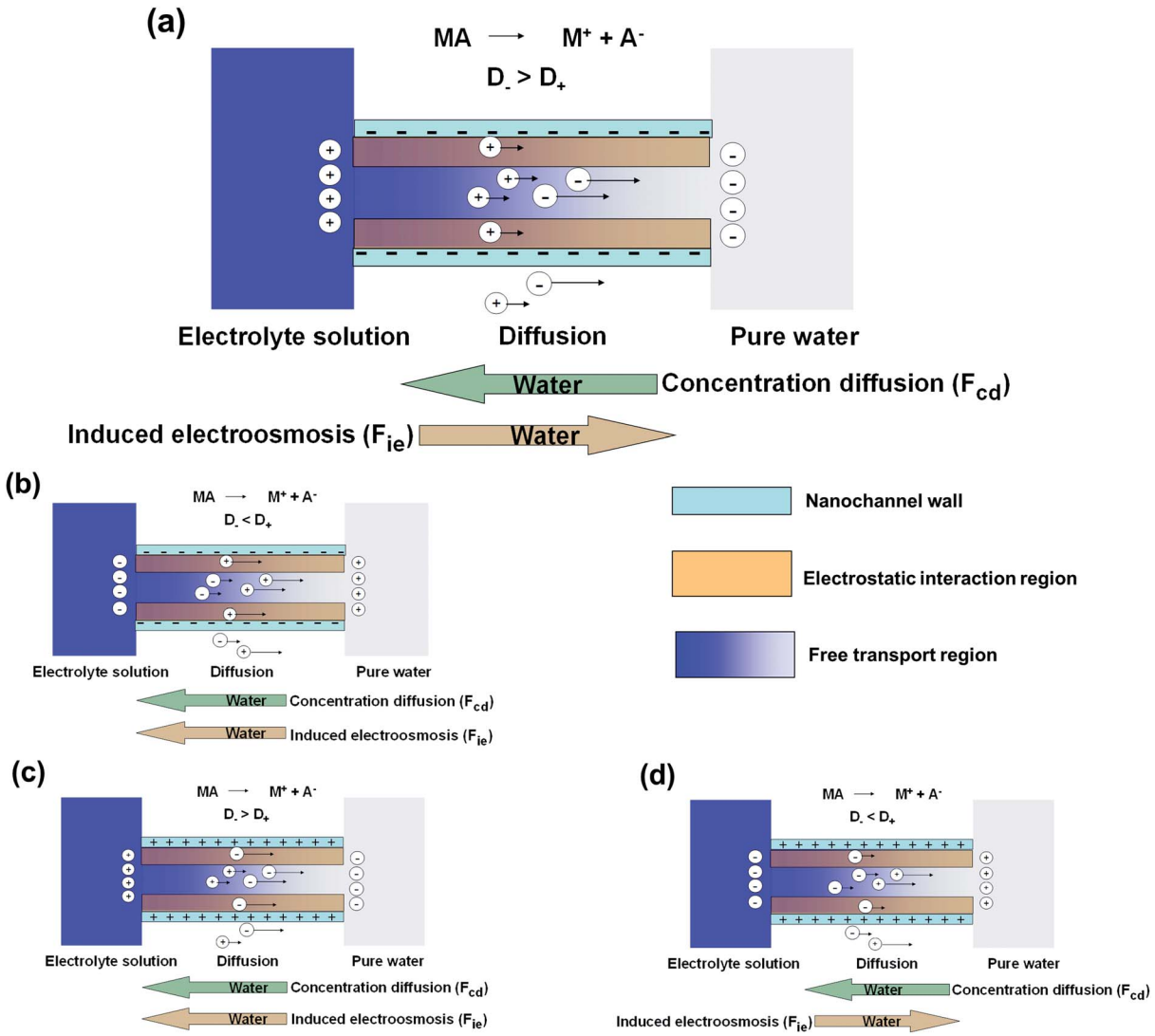

Fig. 1 Schematic of water transport across charged nanochannel membranes. MA, M^+, A^-, D_+ and D_- represent the electrolyte, cation, anion, cation diffusion coefficient and anion diffusion coefficient, respectively; the green arrow represents the direction of water transport induced by electrolyte concentration diffusion, and the orange arrow represents the direction of water transport due to induced electroosmosis.

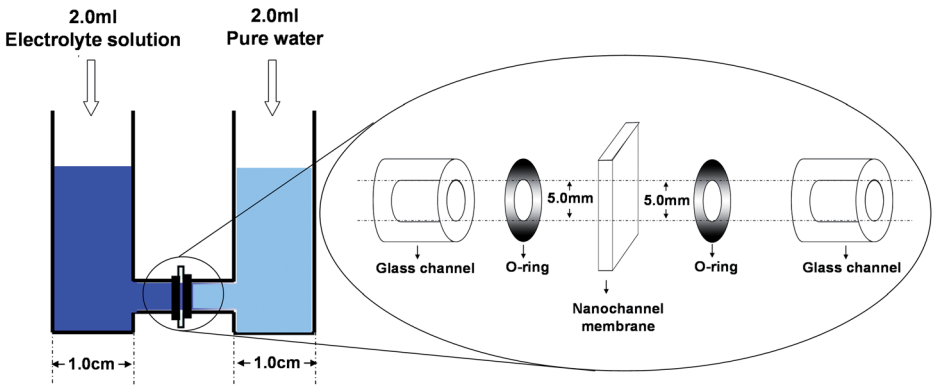

Fig. 2 Schematic representation of the setup for the water transport experiments. The liquid volume of each half-cell was 2.0 mL at the beginning of the experiments.

Published on 09 May 2014. Downloaded by Michigan State University on 23/01/2016 03:02:08.

3 Materials and methods

3.1 Materials

Poly(sodium 4-styrenesulfonate) (PSS) (M_w = 70 000) and poly(allylamine hydrochloride) (PAH) (M_w = 56 000) were purchased from Aldrich and used as received. Methylviologen (MV^{2+}) and 1,5-naphthalene disulfonate (NDS^{2-}) were purchased from TCI and used as received. Phenol, lithium chloride, sodium chloride, potassium chloride, calcium chloride, magnesium chloride, barium chloride, hydrochloric acid, nitrate, sulfuric acid, and phosphate were purchased from Xilong reagent company (Guangdong China). Track-etched polycarbonate membranes (TEPC, 6 μm thickness, 25 mm diameter) whose pore diameters are 100 nm were purchased from Osmonics. All solutions were prepared with ultrapure Milli-Q water (resistance > 18.2 MΩ cm^{-1}).

3.2 Modification of track-etched polycarbonate membranes with polyelectrolyte multilayers

Polyelectrolyte solutions at a concentration of 1 mg mL^{-1} were prepared in 100 mM acetate buffer (pH ~ 4.7) under conditions of full protonation of the PAH. All solutions were freshly prepared before use.[45]

A track-etched polycarbonate membrane was immersed in methanol for 5 min and then immersed for 45 min in a solution that contained 25 mM $SnCl_2$ and 70 mM trifluoroacetic acid. The membrane was then washed in methanol two consecutive times for 2.5 min each.[46] This yielded the Sn-sensitized form of the membrane that was then used for the preparation of the charged nanochannel membrane. This membrane was then placed in a filter holder and polyelectrolyte multilayers were deposited by filtering the polyanion (PSS) solution and the polycation (PAH) solution alternately in vacuum. Each filtration process was repeated three times, and copious amounts of water were used to remove any unabsorbed polymer before next filtering a polyelectrolyte solution. In this way, both negatively and positively charged nanochannels can be obtained.[47]

3.3 Electron microscopy characterization of multilayer nanochannel membranes

To measure the multilayer growth in pores of track-etched polycarbonate membranes, scanning electron microscopy (SEM) and cross-section transmission electron microscopy (TEM) were performed. SEM images were obtained using a JSM-6700 operated at 5.0 kV. For TEM, the membranes were dissolved in dichloromethane with subsequent sonication for less than 30 s. The extracted nanotubes were then collected on TEM carbon grids and imaged with a JEOL-JEM operated at 100 keV.[45]

3.4 Measurement of water flux

To study the transport of water, the membrane was mounted between two half-cells. The experimental setup is schematically depicted in Fig. S4†. Typically, 2.0 mL of electrolyte solution was placed in one half-cell, and 2.0 mL of pure water was placed in the other half-cell, keeping the same liquid level in the two half-cells at the beginning of the experiments.

After 12 h, differences in liquid levels were observed due to water transport. The liquid levels in the two half-cells were measured using a DSA100 Contact Angle Measuring System (KRÜSS) (positioning accuracy = 0.1 mm) (Fig. S4b†).

Then the difference in liquid levels can be converted to net flux of water transport using the equation:

$$J_w = \frac{A_c\left(\frac{\Delta h}{2}\right)\rho}{M_w t A_m} \times 10^6 \quad (1)$$

where J_w is the water flux (μmol min^{-1} cm^{-2}), A_c is the cross sectional area of a half-cell (0.25π cm^2), Δh is the difference in liquid level (cm), ρ is the density of water (1.0 g mL^{-1}), M_w is the molar mass of water (18 g mol^{-1}), t is the penetration time (min), and A_m is the area of nanochannel membrane (π/16 cm^2).

3.5 Measurement of phenol-diffusion flux

The phenol flux was determined by monitoring the concentration change of phenol in the permeation half-cell. This was accomplished by UV detection of the permeation solution with a UV/Vis spectrophotometer (UV-1601, SHIMADZU) at 270 nm. The absorbance data were converted to the concentration of phenol.

The phenol flux was calculated from the experimental data using the equation:

$$J_{PhOh} = \frac{VC_{PhOH}}{tA_m} \times 10^6 \quad (2)$$

where J_{PhOH} is the phenol flux (nmol min^{-1} cm^{-2}), V is the volume of solution in the permeation half-cell (mL), C_{PhOH} is the phenol concentration (mol L^{-1}) in the permeation half-cell, t is the penetration time (min), and A_m is the area of nanochannel membrane (π/16 cm^2).

3.6 Separation of MV^{2+} and NDS^{2-}

The flux of MV^{2+} and NDS^{2-} was determined by monitoring the concentration change of MV^{2+} and NDS^{2-} in the permeation half-cell. This was accomplished by UV detection of the permeation solution with a UV/Vis spectrophotometer (UV-1601, SHIMADZU) at 225 nm and 257 nm. The absorbance data were converted to the concentrations of MV^{2+} and NDS^{2-}.

The flux of MV^{2+} and NDS^{2-} were calculated using the equations:

$$J_{MV^{2+}} = \frac{VC_{MV^{2+}}}{tA_m} \times 10^6 \quad (3)$$

$$J_{NDS^{2-}} = \frac{VC_{NDS^{2-}}}{tA_m} \times 10^6 \quad (4)$$

where $J_{MV^{2+}}$ and $J_{NDS^{2-}}$ are the flux of MV^{2+} and NDS^{2-} (nmol min^{-1} cm^{-2}), respectively, V is the volume of solution in the permeation half-cell (mL), $C_{MV^{2+}}$ and $C_{NDS^{2-}}$ are the concentration of the MV^{2+} and NDS^{2-} (mol L^{-1}), respectively, in the permeation solution after permeating for 3 h, t is the penetration time (min), and A_m is the area of nanochannel membrane (π/16 cm^2).

 This journal is © The Royal Society of Chemistry 2014

Published on 09 May 2014. Downloaded by Michigan State University on 23/01/2016 03:02:08.

4 Results and discussion

4.1 Water transport through 3.5(PSS/PAH) coated 100 nm nanochannel membranes with different LiCl concentrations

According to van't Hoff's law, the electrolyte concentration can affect F_{cd}. The sizes of the electrostatic interaction region and the free transport region in the transport model are also related to the electrolyte concentration. This is because the size of the electric double layer is characterized by the Debye screening length. The ion concentration η and the Debye screening length l_D follow the relationship $l_D \propto 1/\sqrt{\eta}$.[35] Therefore, the electrolyte concentration is an important factor in water transport.

To study the effect of electrolyte concentration on water transport, 3.5(PSS/PAH) coated 100 nm nanochannel membrane, a negatively charged nanochannel membrane, was used, and LiCl was selected because the diffusion coefficient of Cl^- (2.032×10^{-5} cm^2 s^{-1}) is bigger than that of Li^+ (1.029×10^{-5} cm^2 s^{-1}). Solutions of LiCl in the concentration range from 0 to 1000 mM were investigated. The LiCl solution and pure water were separated by a 3.5(PSS/PAH) coated 100 nm nanochannel membrane. The net flux and direction of water transport were determined by measuring the liquid levels in the two half-cells after 12 h. The difference in liquid levels was converted to the net flux of water transport using eqn (1). Fig. 3 shows the net flux and direction of water transport through the nanochannel membranes as a function of the bulk LiCl concentration.

When the bulk LiCl concentration was relatively low, the water was transported from the pure water side towards the LiCl solution side. The net flux of water increased with the increase in LiCl concentration. This was because the electrostatic interaction region was large and the free transport region was small, even nonexistent at relatively low concentrations due to the electric double layer overlap. It was difficult for Cl^- ions to pass through the channels. Water transport was mainly dominated by F_{cd} from pure water to the LiCl solution.

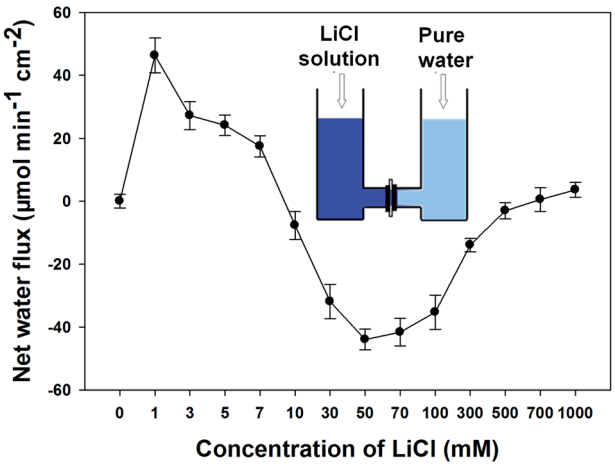

Fig. 3 The net flux of water transport as a function of LiCl concentration. A negative value indicates that the direction of the net flux of water is toward the pure water. The data corresponding to water transport through the 3.5(PSS/PAH) coated 100 nm nanochannel membranes after standing for 12 h at 20 °C.

However, as the bulk LiCl concentration further increased, the net water flux towards the LiCl solution decreased. Once the bulk LiCl concentration exceeded 10 mM, the direction of the net flux of water was changed, and anomalous osmosis was observed. Subsequently, the net water flux towards pure water increased with the increase in LiCl concentration. When the LiCl concentration increased to 50 mM, the net flux of water reached a maximum, and anomalous osmosis was most obvious. This can be explained as follows: as the bulk LiCl concentration further increased, the EDL gradually became thin, and the size of the free transport region gradually increased. Cl^- ions can quickly pass through the channel by the free transport region, and form a membrane diffusional potential. The membrane diffusional potential acting on Li^+ accumulated in the EDL produced F_{ie} towards pure water. Although F_{cd} and F_{ie} increased with the increase of LiCl concentration, the increase of F_{ie} was faster than F_{cd} in this concentration range. As a result of the competition of F_{cd} and F_{ie}, the direction of the net flux of water changed from the LiCl solution to pure water.

Above this optimal value, the net water flux toward pure water decreased as the LiCl concentration increased. Finally the direction of the net flux of water was changed again. This was because water transport was mainly determined by F_{cd} with the increase of LiCl concentration. These results clearly showed that the net flux and direction of water transport can be modulated as a function of LiCl concentration.

4.2 Effect of nanochannel diameter on water transport with a 50 mM LiCl concentration

The above results indicated that the nanochannel diameter has an important effect on water transport, since the size of the free transport region was different for the charged nanochannels of different diameters under the same electrolyte concentration. To investigate the effect of the nanochannel diameter on water transport, different numbers of (PSS/PAH) multilayers were deposited onto 100 nm pore TEPC membranes.

SEM images of the pores at various stages of multilayer deposition showed that the diameter of the pores decreased with the increasing number of multilayers, and no clogging was observed up to 4.5(PSS/PAH) (see Fig. S2†). In order to ascertain that n(PSS/PAH) multilayers were modified through the full length of the nanochannels, 3.5(PSS/PAH) coated 100 nm nanochannel membrane was treated with dichloromethane to liberate the (PSS/PAH) multilayers. The TEM images of the liberated (PSS/PAH) multilayer nanostructures clearly showed that the modified multilayers were assembled in the interior of the nanochannels (see Fig. S3†).

Experiments on water transport through n(PSS/PAH) multilayers ($n = 0$ to 4.5) were conducted under 50 mM LiCl, as shown in Fig. 4. When $n = 3.5$, the net flux of water toward the direction of pure water was the biggest, and the anomalous osmosis was most obvious. This was because the proportions of the electrostatic interaction region and the free transport region were different due to the difference in nanochannel diameter. In the following experiments, the 3.5(PSS/PAH) coated 100 nm

Published on 09 May 2014. Downloaded by Michigan State University on 23/01/2016 03:02:08.

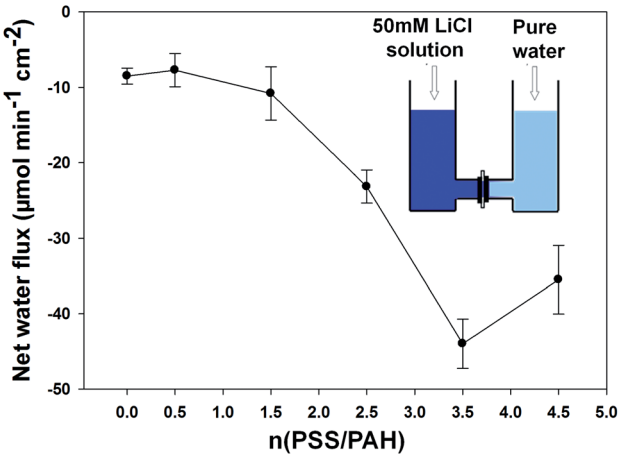

Fig. 4 The net flux of water transport as a function of *n*(PSS/PAH). A negative value indicates that the direction of the net flux of water is toward pure water. The data correspond to water transport through the *n*(PSS/PAH) coated 100 nm nanochannel membranes after standing for 12 h at 20 °C.

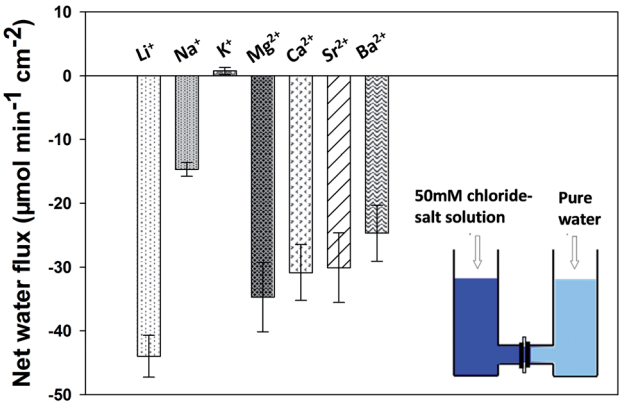

Fig. 5 The net flux of water transport as a function of different electrolyte types. A negative value indicates that the direction of the net flux of water is toward pure water. The data correspond to water transport through the 3.5(PSS/PAH) coated 100 nm nanochannel membranes after standing for 12 h at 20 °C.

nanochannel membranes were selected as the negatively charged nanochannel to study the effects of electrolyte type and non-electrolyte substances on water transport.

4.3 Water transport through 3.5(PSS/PAH) coated 100 nm nanochannel membranes with different electrolyte types

According to the model shown in Fig. 1a, the diffusion coefficient difference of anions (A^-) and cations (M^+) will also affect water transport because the membrane diffusional potential, as the driving force of F_{ie}, is closely related to the diffusion coefficient difference of anions (A^-) and cations (M^+).

To prove this, electrolyte solutions of 50 mM LiCl, NaCl, KCl, $MgCl_2$, $CaCl_2$, $SrCl_2$ and $BaCl_2$ were used for the investigation of water transport. As shown in Fig. 5, the water transport towards pure water gradually decreased from LiCl to NaCl to KCl, and from $MgCl_2$ to $CaCl_2$ to $SrCl_2$ to $BaCl_2$. Obviously, the tendency was the same as that of the difference in the diffusion coefficients shown in Table S1.† The results were consistent with the inference of the transport model shown in Fig. 1a.

Next, electrolyte solutions of 50 mM HCl, HNO_3, H_2SO_4, and H_3PO_4 were used for the investigation of water transport. As shown in Fig. 6, for the 3.5(PSS/PAH) coated 100 nm nanochannel membranes, since the diffusion coefficient of the cation (H^+) was larger than that of the anion (acid radical), the direction of F_{cd} was the same as F_{id}. Water was always transported from pure water toward the acid solution. Anomalous osmosis phenomena could not be observed. These results were consistent with the inference of the model shown in Fig. 1b.

4.4 Water transport through 4.0(PSS/PAH) coated 100 nm nanochannel membranes with different electrolyte types

According to our model, if a positively charged nanochannel membrane was used for water transport under different electrolytes, the inverse situation should be observed.

To prove this, 4.0(PSS/PAH) coated 100 nm nanochannel membranes were selected due to their positively charged surface, and electrolyte solutions of 50 mM LiCl, NaCl, KCl, $MgCl_2$, $CaCl_2$, $SrCl_2$ and $BaCl_2$ were used for the investigation of water transport. As shown in Fig. 7, water was transported from pure water to the chloride–salt solution. The results were the opposite to those of the 3.5(PSS/PAH) coated 100 nm nanochannel membrane, which was consistent with the inference of the model shown in Fig. 1c.

The same situation also occurred when 50 mM HCl, HNO_3, H_2SO_4, and H_3PO_4 were used for the investigation of water transport. As shown in Fig. 8, water was transported from the acid solution to pure water. The results were the opposite to those of 3.5(PSS/PAH) coated 100 nm nanochannel membrane, which was consistent with the inference of the model shown in Fig. 1d.

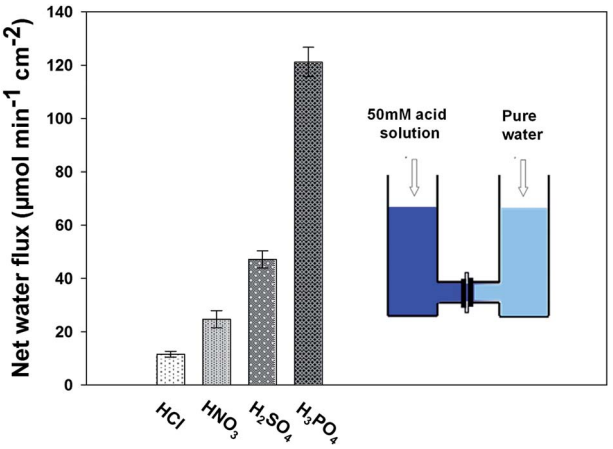

Fig. 6 The net flux of water transport as a function of different electrolyte types. A positive value indicates that the direction of the net flux of water is toward the acid solution. The data correspond to water transport through the 3.5(PSS/PAH) coated 100 nm nanochannel membranes after standing for 12 h at 20 °C.

This journal is © The Royal Society of Chemistry 2014

Published on 09 May 2014. Downloaded by Michigan State University on 23/01/2016 03:02:08.

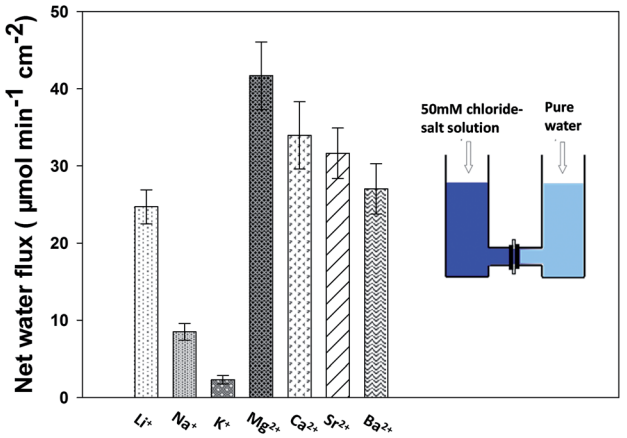

Fig. 7 The net flux of water transport as a function of different electrolyte types. A positive value indicates that the direction of the net flux of water is toward the chloride–salt solution. The data correspond to water transport through the 4.0(PSS/PAH) coated 100 nm nanochannel membranes after standing for 12 h at 20 °C.

4.5 Water transport through 3.5(PSS/PAH) and 4.0(PSS/PAH) coated 100 nm nanochannel membranes with a non-electrolyte solution

According to our model, non-electrolyte substances, which could not be ionized in aqueous solution and form a membrane diffusional potential, should not produce F_{ie} under a concentration gradient. Regardless of the nanochannel surface charge, water transport should be determined by F_{cd} from pure water to the non-electrolyte solution.

To prove this, experiments on water transport through the 3.5(PSS/PAH) and 4.0(PSS/PAH) coated 100 nm nanochannel membranes were performed using 100 mM solutions of glucose and γ-cyclodextrin. The net flux and direction of water transport are given in Fig. 9. Water was transported from pure water toward the non-electrolyte solution. Anomalous osmosis phenomena could not be observed.

4.6 Neutral molecular transport through 3.5(PSS/PAH) coated 100 nm nanochannel membranes under a salt gradient

Modulating and controlling the mass transport across nanochannels is of great importance for designing novel molecular devices, machines and sensors. Here F_{ie} as a form of liquid transport, caused by the interplay of the membrane diffusional potential and EDL, should be useful to modulate neutral molecular transport.

To demonstrate that it is possible to modulate the transport of neutral molecules by F_{ie}, phenol, a neutral molecule commonly used as an indicator in studies of mass-transport behavior in nanochannels,[38] was selected as the model molecule. The flux of phenol was determined by eqn (2). Fig. 10 shows the distinct diffusion behavior of phenol through 3.5(PSS/PAH) coated 100 nm nanochannel membranes under different conditions.

As shown in Fig. 10, in the case of no salt gradient, the diffusion flux of phenol corresponding to condition (b) was larger than that of condition (a). The difference in flux can be explained by the size change of the free transport region and the electrostatic interaction region. When 50 mM LiCl was added, the free transport region expanded while electrostatic interaction region shrank. The expansion of the free transport region facilitated the diffusion of phenol, since the diffusion of phenol was slow in the electrostatic interaction region due to the interaction between the inductive dipole of phenol and the negatively charged surface.[38]

When the salt gradient was established under condition (c), the diffusion flux of phenol further increased compared with condition (b). This can be explained by our model, as shown in Fig. 1a. Under condition (c), the direction of F_{ie} was from the feed half-cell to the permeation half-cell, and the direction of net water flux was toward the permeation half-cell. Therefore, the direction of phenol diffusion was consistent with the direction of F_{ie}, which promoted the transport of phenol through the nanochannel membranes.

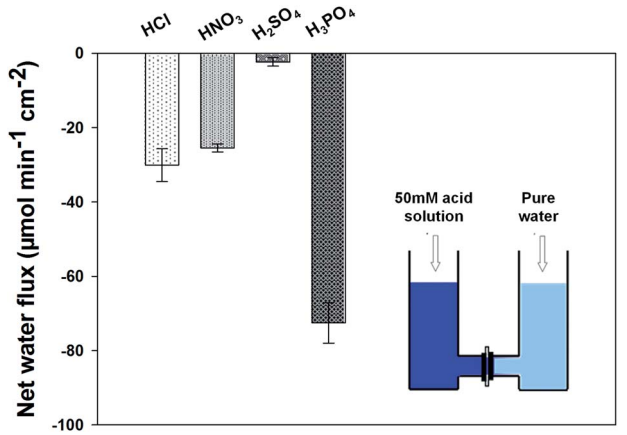

Fig. 8 The net flux of water transport as a function of different electrolyte types. A negative value indicates that the direction of the net flux of water is toward pure water. The data correspond to water transport through the 4.0(PSS/PAH) coated 100 nm nanochannel membranes after standing for 12 h at 20 °C.

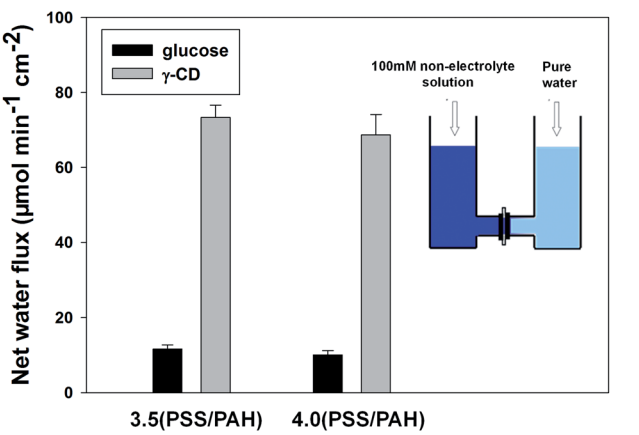

Fig. 9 The net flux of water transport in the presence of non-electrolytes. A positive value indicates that the direction of the net flux of water is toward the non-electrolyte solution The data correspond to water transport through 3.5(PSS/PAH) and 4.0(PSS/PAH) coated 100 nm nanochannel membranes after standing for 12 h at 20 °C.

Published on 09 May 2014. Downloaded by Michigan State University on 23/01/2016 03:02:08.

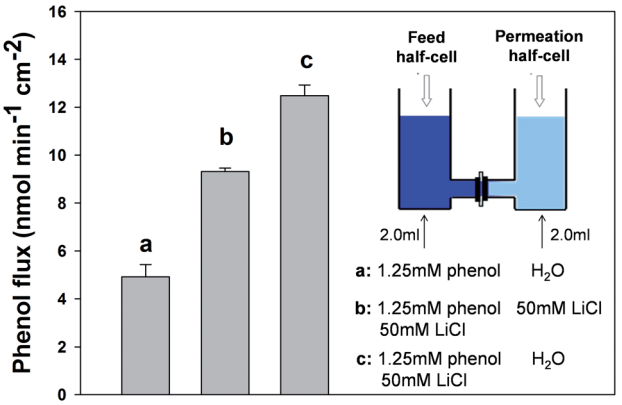

Fig. 10 The net flux of phenol transport through 3.5 (PSS/PAH) coated 100 nm nanochannel membranes after stirring for 3 h at 20 °C. A positive value indicates that the direction of the net flux of phenol is toward the permeation half-cell.

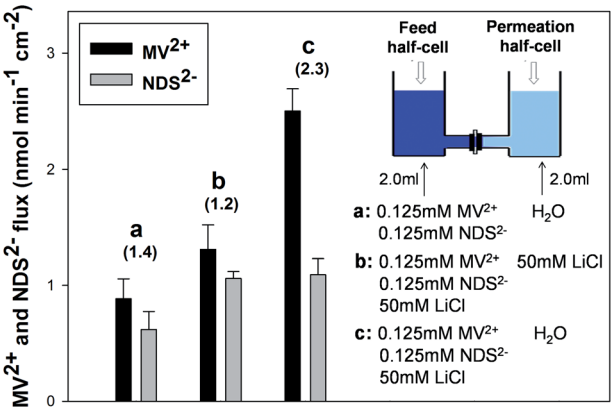

Fig. 11 The net flux of MV^{2+} and NDS^{2-} through 3.5(PSS/PAH) coated 100 nm nanochannel membranes after stirring for 3 h at 20 °C. A positive value indicates that the direction of the net flux of MV^{2+} and NDS^{2-} is toward the permeation half-cell. The data above the histogram correspond to the separation selectivity S of MV^{2+}.

These studies clearly demonstrated that the F_{ie} could be utilized to modulate the transport rate of neutral molecules through the charged nanochannel membranes.

4.7 Separation of ionic species using 3.5(PSS/PAH) coated 100 nm nanochannel membranes under a salt gradient

The permeation of ionic species through charged nanochannel membranes is common in many biophysical systems and biotechnological applications. According to our model, the membrane diffusional potential, caused by the asymmetric diffusion between cations and anions, acted on ionic species leading to induced electrophoresis. This collaboration between induced electroosmosis and induced electrophoresis can be further employed to improve the separation selectivity of different charged molecules.

In order to investigate the effect of the induced electroosmosis and induced electrophoresis on ionic species separation, MV^{2+} and NDS^{2-} were selected as the model cation and anion, since they are both divalent ions and have similar molecular volumes.[48] This ensured that the separation of MV^{2+} and NDS^{2-} was based on charge difference rather than volume difference.

Fig. 11 shows the separation selectivity of the mixed solution of MV^{2+} and NDS^{2-} through 3.5(PSS/PAH) coated 100 nm nanochannel membranes under different conditions. The separation selectivity S was defined as

$$S = \frac{J_{MV^{2+}}}{J_{NDS^{2-}}} \quad (5)$$

where $J_{MV^{2+}}$ and $J_{NDS^{2-}}$ represent the fluxes of MV^{2+} and NDS^{2-}, respectively (see eqn (3) and (4)).

As shown in Fig. 11, in the case of no salt gradient, the diffusion flux of MV^{2+} and NDS^{2-} corresponding to condition (b) was larger than that in the condition (a), but the change of S of MV^{2+} was not obvious. This phenomenon could also be explained by the size change of the free transport region and electrostatic interaction region. When 50 mM LiCl was added, the free transport region expanded, and the flux of MV^{2+} and NDS^{2-} increased from condition (a) to condition (b).

When a salt gradient was established under condition (c), the separation selectivity S further increased. The improvement of separation selectivity could also be explained by our model, as shown in Fig. 1a. Under a salt gradient, a membrane diffusional potential was formed due to the different diffusion of Li^+ and Cl^-. For MV^{2+}, the direction of induced electroosmosis and induced electrophoresis was the same as that of the diffusion. For NDS^{2-}, only the direction of induced electroosmosis was the same as that of the diffusion. Therefore, the flux of MV^{2+} was dramatically higher than that of NDS^{2-}.

The results clearly demonstrated that the membrane diffusional potential could be utilized to improve the separation selectivity of ionic species in charged nanochannel membranes.

5 Conclusions

In summary, we have presented anomalous effects of water flow through charged nanochannel membranes. A concise model was established to describe the conditions of these anomalous effects. According to the model, water transport was composed of concentration diffusion and induced electroosmosis under an electrolyte gradient. The direction and net flux of water transport were sensitive to the nanochannel surface charge, electrolyte concentration and electrolyte type, which was confirmed by experiments. In addition, we have also demonstrated that the transport of electrically neutral molecules and the separation selectivity of ionic species through charged nanochannel membranes can be modulated by adjusting the electrolyte gradient. These results may deepen our understanding of mass transport at the nanoscale and may also be helpful in the development of nanofluidic devices. From the perspective of potential applications, it may be possible for polyelectrolyte modified nanochannel membranes to develop into a kind of nanovalve under electrolyte gradients.

 This journal is © The Royal Society of Chemistry 2014

Published on 09 May 2014. Downloaded by Michigan State University on 23/01/2016 03:02:08.

Acknowledgements

This work was supported by the National Natural Science Foundation of China (21190040, 21175035, 21375034), National Basic Research Program (2011CB911002), International Science & Technology Cooperation Program of china (2010DFB30300).

Notes and references

1 F. Fornasiero, H. G. Park, J. K. Holt, M. Stadermann, C. P. Grigoropoulos, A. Noy and O. Bakajin, *Proc. Natl. Acad. Sci. U. S. A.*, 2008, **105**, 17250–17255.
2 X. J. Gong, J. Y. Li, H. J. Lu, R. Z. Wan, J. C. Li, J. Hu and H. P. Fang, *Nat. Nanotechnol.*, 2007, **2**, 709–712.
3 T. Jovanovic-Talisman, J. Tetenbaum-Novatt, A. S. McKenney, A. Zilman, R. Peters, M. P. Rout and B. T. Chait, *Nature*, 2009, **457**, 1023–1027.
4 P. Stroeve and N. Ileri, *Trends Biotechnol.*, 2011, **29**, 259–266.
5 X. Hou, W. Guo and L. Jiang, *Chem. Soc. Rev.*, 2011, **40**, 2385–2401.
6 Y. H. Zhou, W. Guo and L. Jiang, *Sci. China: Phys., Mech. Astron.*, 2014, **57**, 836–843.
7 L. J. Cheng and L. J. Guo, *Chem. Soc. Rev.*, 2010, **39**, 923–938.
8 J. C. T. Eijkel and A. van den Berg, *Chem. Soc. Rev.*, 2010, **39**, 957–973.
9 W. Sparreboom, A. van den Berg and J. C. T. Eijkel, *Nat. Nanotechnol.*, 2009, **4**, 713–720.
10 M. Tagliazucchi, Y. Rabin and I. Szleifer, *J. Am. Chem. Soc.*, 2011, **133**, 17753–17763.
11 I. Vlassiouk, S. Smirnov and Z. Siwy, *Nano Lett.*, 2008, **8**, 1978–1985.
12 D. Gillespie and S. Pennathur, *Anal. Chem.*, 2013, **85**, 2991–2998.
13 X. C. Xuan, *Electrophoresis*, 2008, **29**, 3737–3743.
14 Q. S. Pu, J. S. Yun, H. Temkin and S. R. Liu, *Nano Lett.*, 2004, **4**, 1099–1103.
15 S. J. Kim, Y. C. Wang, J. H. Lee, H. Jang and J. Han, *Phys. Rev. Lett.*, 2007, **99**, 044501.
16 A. Plecis, R. B. Schoch and P. Renaud, *Nano Lett.*, 2005, **5**, 1147–1155.
17 R. Karnik, R. Fan, M. Yue, D. Y. Li, P. D. Yang and A. Majumdar, *Nano Lett.*, 2005, **5**, 943–948.
18 R. Karnik, K. Castelino and A. Majumdar, *Appl. Phys. Lett.*, 2006, **88**, 123114.
19 R. Fan, S. Huh, R. Yan, J. Arnold and P. D. Yang, *Nat. Mater.*, 2008, **7**, 303–307.
20 K. H. Paik, Y. Liu, V. Tabard-Cossa, M. J. Waugh, D. E. Huber, J. Provine, R. T. Howe, R. W. Dutton and R. W. Davis, *ACS Nano*, 2012, **6**, 6767–6775.
21 H. Zhang, X. Hou, L. Zeng, F. Yang, L. Li, D. Yan, Y. Tian and L. Jiang, *J. Am. Chem. Soc.*, 2013, **135**, 16102–16110.
22 X. Hou, F. Yang, L. Li, Y. Song, L. Jiang and D. Zhu, *J. Am. Chem. Soc.*, 2010, **132**, 11736–11742.
23 Y. Zhou, W. Guo, J. Cheng, Y. Liu, J. Li and L. Jiang, *Adv. Mater.*, 2012, **24**, 962–967.
24 W. J. Lan, D. A. Holden and H. S. White, *J. Am. Chem. Soc.*, 2011, **133**, 13300–13303.
25 M. Ali, B. Yameen, J. Cervera, P. Ramirez, R. Neumann, W. Ensinger, W. Knoll and O. Azzaroni, *J. Am. Chem. Soc.*, 2010, **132**, 8338–8348.
26 R. Karnik, C. H. Duan, K. Castelino, H. Daiguji and A. Majumdar, *Nano Lett.*, 2007, **7**, 547–551.
27 Y. He, D. Gillespie, D. Boda, I. Vlassiouk, R. S. Eisenberg and Z. S. Siwy, *J. Am. Chem. Soc.*, 2009, **131**, 5194–5202.
28 B. Yameen, M. Ali, R. Neumann, W. Ensinger, W. Knoll and O. Azzaroni, *J. Am. Chem. Soc.*, 2009, **131**, 2070–2071.
29 A. Siria, P. Poncharal, A. L. Biance, R. Fulcrand, X. Blase, S. T. Purcell and L. Bocquet, *Nature*, 2013, **494**, 455–458.
30 F. H. J. van der Heyden, D. J. Bonthuis, D. Stein, C. Meyer and C. Dekker, *Nano Lett.*, 2006, **6**, 2232–2237.
31 W. Guo, L. X. Cao, J. C. Xia, F. Q. Nie, W. Ma, J. M. Xue, Y. L. Song, D. B. Zhu, Y. G. Wang and L. Jiang, *Adv. Funct. Mater.*, 2010, **20**, 1339–1344.
32 J. K. Holt, H. G. Park, Y. M. Wang, M. Stadermann, A. B. Artyukhin, C. P. Grigoropoulos, A. Noy and O. Bakajin, *Science*, 2006, **312**, 1034–1037.
33 J. Chmiola, G. Yushin, Y. Gogotsi, C. Portet, P. Simon and P. L. Taberna, *Science*, 2006, **313**, 1760–1763.
34 K. P. Lee, H. Leese and D. Mattia, *Nanoscale*, 2012, **4**, 2621–2627.
35 C. H. Duan and A. Majumdar, *Nat. Nanotechnol.*, 2010, **5**, 848–852.
36 H. Chinen, K. Mawatari, Y. Pihosh, K. Morikawa, Y. Kazoe, T. Tsukahara and T. Kitamori, *Angew. Chem., Int. Ed.*, 2012, **51**, 3573–3577.
37 T. Tsukahara, A. Hibara, Y. Ikeda and T. Kitamori, *Angew. Chem., Int. Ed.*, 2007, **46**, 1180–1183.
38 W. Chen, Z. Q. Wu, X. H. Xia, J. J. Xu and H. Y. Chen, *Angew. Chem., Int. Ed.*, 2010, **49**, 7943–7947.
39 J. Cervera, V. Garcia-Morales and J. Pellicer, *J. Phys. Chem. B*, 2003, **107**, 8300–8309.
40 S. Z. Qian, B. Das and X. B. Luo, *J. Colloid Interface Sci.*, 2007, **315**, 721–730.
41 R. Qiao, J. G. Georgiadis and N. R. Aluru, *Nano Lett.*, 2006, **6**, 995–999.
42 M. Nagasawa, M. Tasaka and M. Tomita, *Neurosci. Lett.*, 1986, **66**, 19–24.
43 S. Hamann, J. J. Herrera-Perez, T. Zeuthen and F. J. Alvarez-Leefmans, *J. Physiol.*, 2010, **588**, 4089–4101.
44 S.-J. Li, J. Li, K. Wang, C. Wang, J.-J. Xu, H.-Y. Chen, X.-H. Xia and Q. Huo, *ACS Nano*, 2010, **4**, 6417–6424.
45 C. J. Roy, C. Dupont-Gillain, S. Demoustier-Champagne, A. M. Jonas and J. Landoulsi, *Langmuir*, 2009, **26**, 3350–3355.
46 K. B. Jirage, J. C. Hulteen and C. R. Martin, *Anal. Chem.*, 1999, **71**, 4913–4918.
47 E. N. Savariar, K. Krishnamoorthy and S. Thayumanavan, *Nat. Nanotechnol.*, 2008, **3**, 112–117.
48 S. B. Lee and C. R. Martin, *Anal. Chem.*, 2001, **73**, 768–775.